ELSEVIER

Biophysical Chemistry 97 (2002) 29–44

Biophysical Chemistry

www.elsevier.com/locate/bpc

Fluorescence pattern photobleaching recovery for samples with multi-component diffusion

Tammy E. Starr[1], Nancy L. Thompson*

Department of Chemistry, Campus Box 3290, University of North Carolina at Chapel Hill, Chapel Hill, NC 27599-3290, USA

Received 16 November 2001; received in revised form 8 February 2002; accepted 8 February 2002

Abstract

The translational mobility of proteins and lipids in phospholipid bilayers is often not well described as ideal self diffusion. One of the best methods for characterizing such non-ideal diffusion is to use fluorescence pattern photobleaching recovery. In this method, the spatial gradient of the monitoring and bleaching intensity is created by using epi-fluorescence and an expanded Gaussian-shaped laser beam which passes though a Ronchi ruling placed at the back image plane of a microscope. A difficulty arises when the fluorescence recovery from the exchange of slowly diffusing molecules between illuminated and non-illuminated stripes temporally overlaps with the recovery from the exchange of more rapidly diffusing molecules through the gradient produced by the broad Gaussian shape of the illumination. In the work presented here, a general theory is developed that describes the shape of the resulting fluorescence recovery curve for these typical experimental conditions. Approximate expressions amenable to non-linear curve fitting are also given. The new theoretical formalism has been demonstrated on data for the translational mobility of a fluorescent lipid probe in phospholipid bilayers deposited on planar-fused silica substrates.

Keywords: Lateral mobility; Surface diffusion; Phospholipid bilayers; Supported planar membranes; Fluorescence microscopy

1. Introduction

Fluorescence photobleaching recovery is widely used as a method for examining the translational mobilities of fluorescent lipids or proteins in natural and model membranes [1–5]. In one form of this technique, a focused laser beam is used to create a small bleached and monitored area [6,7]. In an alternative form, called fluorescence pattern photobleaching recovery (FPPR), an expanded laser beam is passed through a ruling in a back image plane to create a broadly illuminated area containing stripes with a well-defined spatial period [8,9].

The lateral mobility of lipids and proteins in phospholipid bilayers is often not well described as ideal self diffusion [10–13]. In these cases, it is of interest to characterize the non-idealities in the diffusive behavior. A common phenomenolog-

*Corresponding author. Tel.: +1-919-962-0328; fax: +1-919-966-3675.

E-mail address: nlt@unc.edu (N.L. Thompson).

[1] Present address: Cellomics, Inc., 635 William Pitt Way, Pittsburgh, PA 15238, USA.

0301-4622/02/$ - see front matter
PII: S0301-4622(02)00037-6

ical approach is to describe the system as containing a discrete number of fluorophore populations, each of which exhibit ideal diffusion, but with different coefficients. However, it is difficult to measure the different apparent diffusion coefficients by using fluorescence photobleaching recovery with a focused spot. The spatial profile of the excitation intensity can deviate from the ideal Gaussian shape of a focused beam after passing through the optical components necessary to create the focused beam, and the form of the fluorescence recovery data depends critically on the beam shape. The spatial profile of the excitation intensity in FPPR is more accurately known, and this method is, therefore, more amenable to quantitatively examining non-ideal diffusion in membrane environments.

There is a difficulty that arises when using FPPR to quantitatively examine non-ideal diffusion. In practice, the beam cannot be infinitely expanded because the intensity becomes so low that effective bleaching cannot be accomplished in a short enough time. In this case, for samples containing both rapidly and slowly mobile components, recovery is observed not only from the exchange of bleached and unbleached molecules between the illuminated and non-illuminated stripes, but also from the exchange of bleached and unbleached molecules from within and without the illuminated area. In this work, we present the theory necessary for analyzing data in this type of sample. The results are illustrated with recovery curves obtained for fluorescent lipid diffusion in planar membranes supported on fused silica. The results have also been used to describe the translational mobility of fluorescent lipids in phospholipid bilayers deposited on high refractive index substrates [14].

2. Theoretical results

2.1. Definitions

We consider a two-dimensional sample (e.g., a supported phospholipid bilayer) containing fluorophores that undergo ideal diffusion with coefficient D. The time-dependent fluorescence is:

$$F(t)=Q\int_{-\infty}^{\infty}\int_{-\infty}^{\infty}I(x,y)C(x,y,t)\mathrm{d}x\,\mathrm{d}y \tag{1}$$

where Q is a proportionality constant, $I(x,y)$ is the monitoring intensity, and $C(x,y,t)$ is the density of unbleached molecules at position (x,y) and time t. For a Gaussian-shaped laser beam intersected by a Ronchi ruling in a back image plane, the intensity can be written as:

$$I(x,y)=\frac{I_0}{2}\exp\left[-\frac{2(x^2+y^2)}{s^2}\right]\times\left[1+\sum_{n\ \mathrm{odd}}c_n\cos(nkx)\right] \tag{2}$$

where I_0 is the intensity at the origin, s is the $1/e^2$-radius of the expanded beam, k is the spatial frequency of the striped pattern:

$$k=\frac{2\pi}{a}\qquad c_n=\frac{4}{n\pi}(-1)^{(n-1)/2} \tag{3}$$

and a is the spatial period. The shape of $I(x,0)$ is illustrated in Fig. 1a. For ideal diffusion:

$$C(x,y,t)=\frac{1}{4\pi Dt}\int_{-\infty}^{\infty}\int_{-\infty}^{\infty}C(x',y',0)\times\exp\left[-\frac{(x-x')^2+(y-y')^2}{4Dt}\right]\mathrm{d}x'\,\mathrm{d}y' \tag{4}$$

The initial density of unbleached molecules can be approximated as [6]:

$$C(x,y,0)=Ce^{-\kappa I(x,y)} \tag{5}$$

where C is the total fluorophore density (bleached plus unbleached) and κ is a constant proportional to the bleach pulse duration, the absorptivity of the fluorophores, and the quantum efficiency for bleaching.

2.2. General solution

By using Eqs. (2), (4) and (5) in Eq. (1), one finds that (see Appendix A)

$$F(t)=\frac{QI_0C\pi s^2}{4}\left[1+h_0+\sum_{i=1}^{5}h_i(t)\right] \tag{6}$$

where

$$h_0 = \sum_{n\ \mathrm{odd}} c_n \exp[-n^2\sigma]$$

$$h_1(t) = \sum_{p=1}^{\infty} \frac{(-\alpha)^p}{2p![1+p(1+2\lambda t)]}$$

$$h_{2,3}(t) = \sum_{p=1}^{\infty} \sum_{n\ \mathrm{odd}} \frac{c_n(-\alpha)^p}{2p![1+p(1+2\lambda t)]} \exp\left[-\frac{1+2(1,p)\lambda t}{1+p(1+2\lambda t)} n^2\sigma\right]$$

$$h_{4,5}(\mathrm{t}) = \sum_{p=1}^{\infty} \sum_{m,n\ \mathrm{odd}} \frac{c_m c_n(-\alpha)^p}{4p![1+p(1+2\lambda t)]} \exp\left[-\frac{(m\pm n)^2+(m^2+pn^2)2\lambda t}{1+p(1+2\lambda t)}\sigma\right] \quad (7)$$

and

$$\alpha = \kappa I_0 \qquad \sigma = \frac{(ks)^2}{8} \qquad \lambda = \frac{4D}{s^2} \quad (8)$$

The dimensionless parameter σ describes the relative size of the Gaussian beam and the striped pattern. When σ is small, the stripe period is high relative to the beam size. This condition corresponds to conventional fluorescence photobleaching recovery with a focused laser beam [6,7]. When σ is large, the stripe period is low relative to the beam size. This condition corresponds to conventional FPPR with a Ronchi ruling [8,9]. The characteristic rates for diffusion through the Gaussian beam and the stripe period are λ and $2\sigma\lambda = k^2D$, respectively.

The fluorescence before photobleaching, $F(-)$, is found by using Eqs. (1) and (2) with $C(x,y,t) = C$. One finds that:

$$F(-) = \frac{QI_0C\pi s^2}{4}(1+h_0) \quad (9)$$

where h_0 is defined in Eq. (7). As shown in Fig. 1b, the pre-bleach fluorescence decreases from $QI_0C\pi s^2/2$ (for low σ) to $QI_0C\pi s^2/4$ (for high σ).

The fraction of the initial fluorescence which is bleached, denoted as β, is equal to [see Eqs. (6) and (7), and Appendix A]:

$$\beta = 1 - \frac{F(0)}{F(-)} = -\sum_{p=1}^{\infty} \frac{(-\alpha)^p}{(p+1)!} \frac{1+\sum_{n\ \mathrm{odd}} c_n e^{-[n^2\sigma/(p+1)]}}{1+\sum_{n\ \mathrm{odd}} c_n e^{-n^2\sigma}} \quad (10)$$

This parameter, which increases from zero to one with α is shown in Fig. 1c,d. When $\sigma = 0$ or $\sigma \to \infty$,

$$[\beta]_{\sigma=0,\sigma\to\infty} = -\sum_{p=1}^{\infty} \frac{(-\alpha)^p}{(p+1)!} = \frac{e^{-\alpha}-1+\alpha}{\alpha} \quad (11)$$

2.3. Limit of no ruling

When the ruling is not present, $\sigma = 0$, and Eqs. (6), (7) and (9) reduce to:

$$\frac{F(t)}{F(-)} = \sum_{p=0}^{\infty} \frac{(-\alpha)^p}{(p+1)!} \frac{1}{1+\lambda_p t} \qquad \lambda_p = \frac{2p\lambda}{1+p} \quad (12)$$

Eq. (12) agrees with the previously published expression for fluorescence photobleaching recovery with a focused laser beam [6]. As shown in Fig. 2, for a bleach depth of $\beta = 0.8$, the infinite sum is sufficiently approximated by retaining the $p = 0$ to 16 terms.

2.4. Limit of infinite Gaussian beam

When the $1/e^2$-width of the Gaussian beam approaches infinity, $\sigma \to \infty$ and $\lambda \to 0$ while $2\sigma\lambda$ remains finite and equal to k^2D. In this case, h_0 and $h_i(t)$ for $i = 2$–4 are zero [Eq. (7)]. In addition, the terms in $h_5(t)$ are zero except when $m = n$. Of these terms, only those with $n = 1$ or $n = 3$ are of non-negligible magnitude. Eqs. (6), (7) and (9) reduce to:

$$\frac{F(t)}{F(-)} = 1 - \frac{\beta}{2} \times \left[1 + \frac{8}{\pi^2}\left(e^{-K^2Dt} + \frac{1}{9}e^{-9K^2Dt}\right)\right] \quad (13)$$

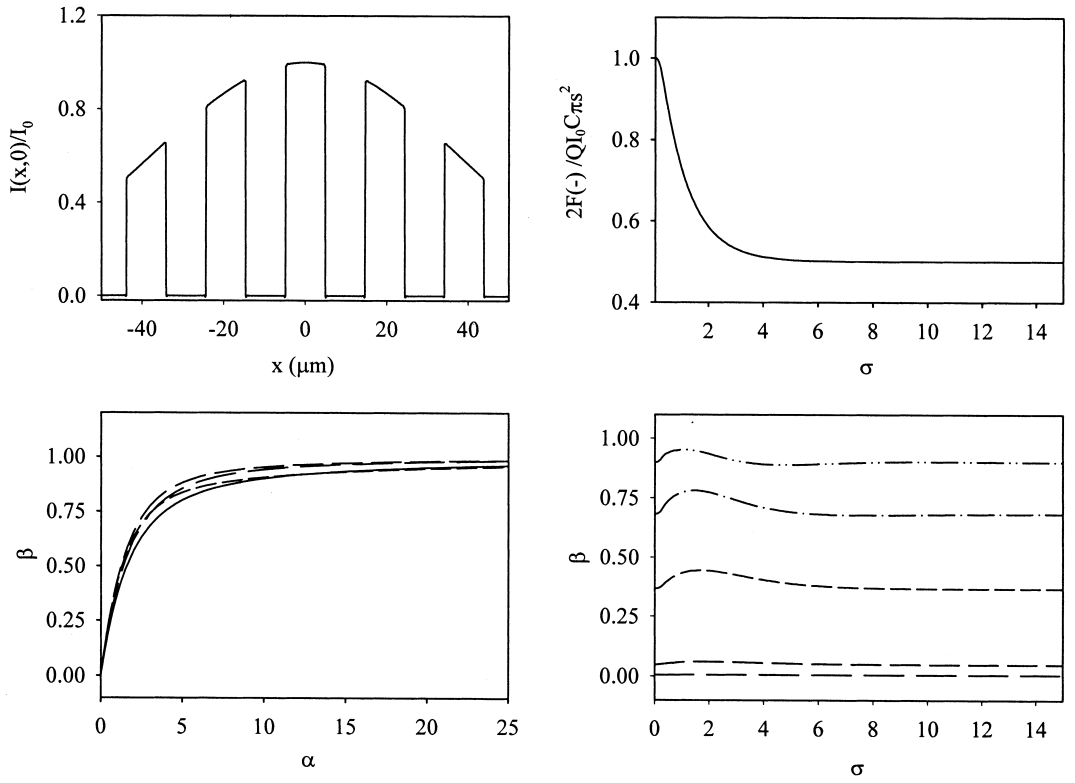

Fig. 1. Spatial intensity profile, pre-bleach fluorescence and bleach depth. (a) $I(x,0)/I_0$ was calculated from Eqs. (2) and (3) for the typical experimental parameters of $s=75$ μm and $a=19.5$ μm. (b) The quantity $[2F(-)]/[QI_0C\pi s^2]$ was calculated by using Eqs. (3), (7) and (9), and ranges from 1 when $\sigma=0$ (no ruling) to 1/2 when $\sigma\rightarrow\infty$ (ruling period much smaller than the Gaussian beam). (c) The bleaching depth β was calculated by using Eq. (10) and is shown as a function of α for σ equal to 0.5 (long dash), 1 (intermediate dash) and 3 (short dash). For small or large values of σ, β is given by Eq. (11) (line). (d) The bleaching depth β was calculated by using Eq. (10) and is shown as a function of σ for α equal to 0.01 (long dash), 0.1 (intermediate dash), 1 (short dash), 3 (dash–dot) and 10 (dash–dot–dot).

where β is given by Eq. (11). This expression agrees with previously published forms[2] [8,15,16]. At time 'infinity', $F(t)/F(-)$ approaches $1-\beta/2$ rather than one. When the ruling is removed, $k=0$ and $F(t)/F(-)=1-\beta$ (no recovery).

2.5. Limit of large Gaussian beam

For many experimental conditions, the $1/e^2$-width of the Gaussian beam is larger than the ruling period, but some recovery still occurs via diffusion through the shape of the Gaussian beam. In this case, an applicable expression for the fluorescence recovery can be found by considering the form of Eqs. (6), (7) and (9) when $\sigma>1$ and $\lambda t<2$. For these conditions, numerical calculations show that the functions h_0 and $h_i(t)$ for $i=2$–5 [Eqs. (6) and (7)] are of negligible magnitude except for the $h_5(t)$ with $m=n=1$ or $m=n=3$. The parameter β is given approximately by Eq. (11) (Fig. 1) and:

$$\frac{F(t)}{F(-)}=1+\frac{1}{2}\sum_{p=1}^{\infty}\frac{(-\alpha)^p}{(p+1)!}\frac{1}{1+\lambda_p t}\times\left[1+\frac{8}{\pi^2}\left(e^{-K^2Dt/(1+\lambda_p t)}+\frac{1}{9}e^{-9K^2Dt/(1+\lambda_p t)}\right)\right] \quad (14)$$

[2] A typographical error is present in Eq. 1 in reference 16. The negative sign preceding the factor (1/9) should be a positive sign.

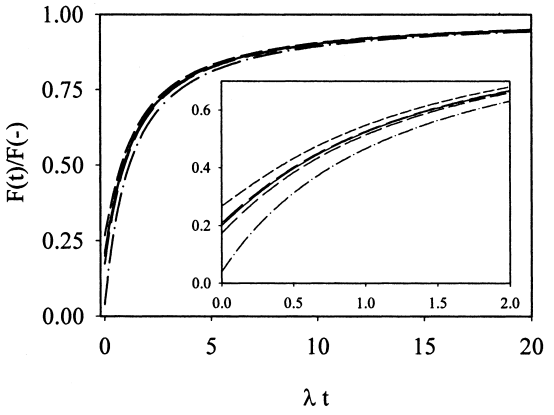

Fig. 2. Approximate forms for theoretical shapes for fluorescence recovery curves. $F(t)/F(-)$ was calculated with the expression in Eq. (12) summed over $p=0$–9 (dash–dot); $p=$ 0–10 (short dash); $p=0$–11 (intermediate dash); $p=0$–12 (long dash); and $p=0$ to ≥ 16 (line). For these plots, $\sigma=0$. The parameter α was set equal to 5.0 so that the bleached fraction β was 0.8 [Eq. (11)]. Similar results were found for Eqs. (14) and (16).

where λ_p is given in Eq. (12). Similar expressions have been reported previously [17]. When the ruling is removed, $k=0$ and Eq. (14) reduces to Eq. (12). When the beam area is very large, $s\rightarrow\infty$, $\lambda_p\rightarrow 0$, and Eq. (14) reduces to Eq. (13). For typical experimental conditions, numerical calculations show that the terms for $p=1$–16 must be retained for adequate sum convergence in Eq. (14).

2.6. Samples containing species with similar diffusion coefficients and an immobile species

Some samples can be described as containing a number of discrete species with similar diffusion coefficients as well as an immobile species, although the data must have a high signal-to-noise ratio to detect this condition. For the typical experimental situation in which $\sigma\rightarrow\infty$, Eq. (13) implies that [16]:

$$\frac{F(t)}{F(-)}=1-\beta+\frac{\beta}{2}\sum_{i=1}^{q}\mu_i\left[1-\frac{8}{\pi^2}\times\left(e^{-K^2D_it}+\frac{1}{9}e^{-9K^2D_it}\right)\right] \quad (15)$$

where μ_i is the fraction of the pre-bleach fluorescence arising from molecules of the ith species, D_i is the diffusion coefficient of the ith species, q is the number of mobile species, and it has been assumed that all species bleach with equal efficiency. At time zero, $F(t)/F(-)=1-\beta$. At longer times, the normalized fluorescence recovery curve plateaus at $1-\beta+\beta(\mu_1+\mu_2+\ldots+\mu_q)/2$.

2.7. Samples with rapidly mobile, slowly mobile and immobile species

Given the typical signal-to-noise ratio of fluorescence photobleaching recovery curves and the intrinsic heterogeneity of many samples, a common condition is that the samples can best be described as containing a rapidly diffusing species (D_1), a slowly diffusing species ($D_2\approx D_1/10$), and an immobile species. To accurately measure D_2, the data acquisition time must be extended into the range where recovery arising from diffusion of the rapidly mobile species through the $1/e^2$-radius of the Gaussian beam is not negligible. Allowing λ_p for the slowly diffusing species to approach zero, one finds that [Eqs. (13) and (14)]:

$$\frac{F(t)}{F(-)}=1+\sum_{p=1}^{\infty}\frac{(-\alpha)^p}{(p+1)!}\times\left\{1-\frac{\mu_2}{2}\left[1-\frac{8}{\pi^2}\left(e^{-K^2D_2t}+\frac{1}{9}e^{-9K^2D_2t}\right)\right]-\frac{\mu_1}{2}\left[2-\frac{1}{(1+\lambda_pt)}\times\left\{1+\frac{8}{\pi^2}\left(e^{-K^2D_it/(1+\lambda_pt)}+\frac{1}{9}e^{-9K^2D_it/(1+\lambda_pt)}\right)\right\}\right]\right\} \quad (16)$$

where μ_i is the fraction of the pre-bleach fluorescence arising from molecules of the ith species and λ_p is given by Eqs. (8) and (12) with $D=D_1$. Numerical calculations show that Eq. (16) adequately converges when the terms for $p=1$–16 are retained. In Eq. (16), $F(0)/F(-)=1-\beta$; over longer times, $F(t)/F(-)\rightarrow 1-\beta+\beta(\mu_1+\mu_2)/2$. When $\lambda_p\rightarrow 0$, Eq. (16) reduces to Eq. (15) with $q=2$. When the ruling is not present, $k=0$, and Eq. (16) reduces to:

$$\left[\frac{F(t)}{F(-)}\right]_{k=0}=\sum_{p=0}^{\infty}\frac{(-\alpha)^p}{(p+1)!}\frac{1+(1-\mu_1)\lambda_pt}{1+\lambda_pt} \quad (17)$$

When $\mu_1 = 1$, Eq. (17) reduces to Eq. (12).

2.8. Limit of low bleaching depths

Eqs. (16) and (17) are significantly more simple in the limit of shallow bleaching ($\alpha \ll 1$) where only the $p = 1$ term is required:

$$\frac{F(t)}{F(-)} = 1 - \frac{\alpha}{2}\left\{1 - \frac{\mu_2}{2}\left[1 - \frac{8}{\pi^2}\left(e^{-K^2 D_2 t} + \frac{1}{9}e^{-9K^2 D_2 t}\right)\right] - \frac{\mu_1}{2}\left[2 - \frac{1}{(1+\lambda t)}\left\{1 + \frac{8}{\pi^2} \times \left(e^{-K^2 D_1 t/(1+\lambda_p t)} + \frac{1}{9}e^{-9K^2 D_1 t/(1+\lambda_p t)}\right)\right\}\right]\right\} \quad (18)$$

where λ is given by Eq. (8) with $D = D_1$. At time zero, $F(0)/F(-) = 1 - \alpha/2$ [Eq. (11) with $\alpha \ll 1$ and $p = 1$; $\beta = \alpha/2$). At long times, $F(t)/F(-) \rightarrow 1 - (\alpha/2)(1 - \mu_1 - \mu_2/2)$. In the absence of the ruling ($k = 0$), Eq. (18) reduces to:

$$\left[\frac{F(t)}{F(-)}\right]_{k=0} = 1 - \frac{\alpha}{2}\frac{1 + (1-\mu_1)\lambda t}{1 + \lambda t} \quad (19)$$

Furthermore, when $\lambda t \ll 1$:

$$\left[\frac{F(t)}{F(-)}\right]_{k=0, \lambda t \ll 1} = 1 - \frac{\alpha}{2} + \frac{\alpha}{2}\mu_1 \lambda t. \quad (20)$$

3. Materials and methods

3.1. Substrate-supported phospholipid bilayers

Substrate-supported planar phospholipid bilayers were formed as previously described [14]. Fused silica substrates (25×25×1 mm) (Quartz Scientific, Fairport Harbor, OH, USA) were cleaned by boiling in detergent (Lot 08778, ICN, Aurora, OH, USA), bath sonicating, rinsing thoroughly with deionized water, and drying at 160 °C. Immediately before bilayer deposition, substrates were cleaned in an argon ion plasma cleaner (15 min, 25 °C) (PDC-3XG, Harrick Scientific, Ossining, NY, USA). Small unilamellar vesicles composed of 1-palmitoyl-2-oleoyl-sn-glycero-3-phospocholine(POPC), cholesterol, and 1-acyl-2-[12-[(7-nitro-2-1,3-benzoxadiazol-4-yl)amino] dodecanoyl]-sn-glycero-3-phosphocholine (NBD-PC) (Avanti Polar Lipids, Birmingham, AL, USA) were prepared. Suspensions containing 2 mM POPC/NBD-PC (98:2, mol/mol) or POPC/cholesterol/NBD-PC (68:30:2, mol/mol/mol) in deionized water were tip sonicated to form vesicles. The vesicle suspensions were then clarified by centrifugation at 130 000×g for 30 min. Planar bilayers were formed by applying 65 μl of the vesicle suspensions to the substrates (30 min, 25 °C), reapplying 65 μl of the vesicle suspensions to the substrates (1 h, 25 °C), and rinsing with 3 ml Tris buffer (0.05 M, pH 7.4).

3.2. Fluorescence pattern photobleaching recovery

Photobleaching measurements were carried out on an instrument consisting of an argon ion laser (Innova 90-3; Coherent, Palo Alto, CA, USA), an inverted optical microscope (Zeiss Axiovert 35), and a single-photon counting photomultiplier (31034A; RCA, Lancaster, PA, USA). The $1/e^2$ beam radius was measured with a CCD (KAF-1400, Photometrics, Tucson, AZ, USA) to be 75 μm when a beam expander (5×, Oriel Corp., Stratford, CT, USA) was placed in the beam path, or 50 μm in the absence of the beam expander. A series of parallel stripes was created by placing a Ronchi ruling (50 lines per inch) in a back image plane, resulting in a ruling periodicity in the sample plane of $a = 19.5$ μm. Other experimental parameters were as follows: excitation wavelength, 488.0 nm; objective, 40× 0.75 N.A.; observation power, 0.3–5 μW; bleach power, 0.5 W; bleach pulse duration, 50–250 ms; and bleach depths, 60–80%. Fluorescence recovery was monitored for 35 or 300 s after photobleaching, and data were curve-fitted to theoretical forms by using the Mathematica (Wolfram Research Inc., Champaign, IL, USA) software package with Global Optimization (Loehle Enterprises, Naperville, IL, USA). The fit parameters were constrained to ensure that the best-fit values obtained were within experimental limitations ($0 \le \mu_{1,2} \le 1$, $\mu_1 + \mu_2 \le 1$ and $0 \le \beta \le 1$) and consistent with the theoretical models ($D_1 \ge D_2$).

4. Experimental results

4.1. General comments

Previous work has suggested that when lipid bilayers are deposited onto fused silica substrates by vesicle adsorption and fusion, the fluorescent lipid NBD-PC undergoes apparent single-component diffusion when the vesicles are composed of POPC and a high molar fraction of cholesterol, whereas NBD-PC exhibits diffusional non-idealities when the vesicles are composed purely of POPC [14]. These two sample types have been used in this work to illustrate the applicability of the theoretical results and to outline methods by which these results can be used to analyze the diffusional properties of fluorescent molecules in two-dimensional samples as measured by FPPR.

4.2. FPPR data

Typical recovery curves for membranes composed of POPC/cholesterol/NBD-PC or POPC/NBD-PC are shown in Figs. 3 and 4, respectively. Data were acquired on both sample types, for acquisition times of 35 s or 5 min, for two beam sizes, and in the presence ($a=19.5$ μm) or absence ($a\rightarrow\infty$ or $k=0$) of the ruling. As shown, the characteristic rate of recovery is slower for the fluorescent lipid in cholesterol-containing samples than for samples containing only POPC. Recovery due to the exchange of bleached molecules from within the observation area with unbleached molecules from outside the observation area is more significant for the smaller observation area than the larger for both sample types. Similarly, this recovery is more significant for POPC samples than for cholesterol-containing samples due to the faster diffusion of the fluorescent lipid in samples without cholesterol. For all conditions, the fluorescence was stable over the acquisition time in the absence of the bleach pulse.

4.3. Analysis of FPPR data using the expressions for a beam of infinite extent

FPPR recovery curves were fit to Eq. (15) with $q=1$ and β, μ_1 and D_1 as free parameters (Fig. 5a,b and Fig. 6a,b). For six of the eight experimental conditions (two membrane compositions, two beam sizes, and two acquisition times), this theoretical form did not adequately fit the data as indicated by large values of χ^2_{red} (>1). Only for cholesterol-containing membranes observed over the shorter acquisition time (35 s) were the values of χ^2_{red} acceptably small (Table 1). FPPR recovery curves were also fitted to Eq. (15) with $q=2$ and β, D_1, D_2, μ_1 and μ_2 as free parameters (Fig. 5c,d and Fig. 6c,d). *F*-statistic analysis determined that this theoretical form, which introduces a second mobile component, was not justified for cholesterol-containing membranes observed over the shorter acquisition time ($F<3$) [16]. This further confirms that Eq. (15) with $q=1$ adequately describes these data. FPPR curves representing POPC membranes observed over the shorter acquisition time were fit well by this model as indicated by the low χ^2_{red} values reported in Table 1. Similarly, *F*-statistic analysis yielded $F\gg 3$, indicating that the use of the two-component model is justified when compared to the single component model for these data. On the contrary, this model did not adequately fit any of the data observed over the longer acquisition time (5 min). Here, χ^2_{red} values were in the range 1.0–1.8, where higher values correspond to samples with faster diffusion and/or smaller observation areas. The reason the theoretical form representing an infinite Gaussian beam shape does not accurately describe the long-time data is that the exchange of bleached molecules with unbleached molecules through the intensity gradient of the Gaussian shape is no longer negligible with longer acquisition times. This exchange is evidenced by the fluorescence recovery in the absence of the ruling (Fig. 3c,d and Fig. 4c,d) and by the observation that the fluorescence recovery in the presence of the ruling is greater than one-half the bleached fluorescence.

4.4. Low bleach approximation

To accurately describe the recovery curves for the remaining four experimental conditions (longer acquisition times), it was necessary to apply a model that accounts for fluorescence recovery from

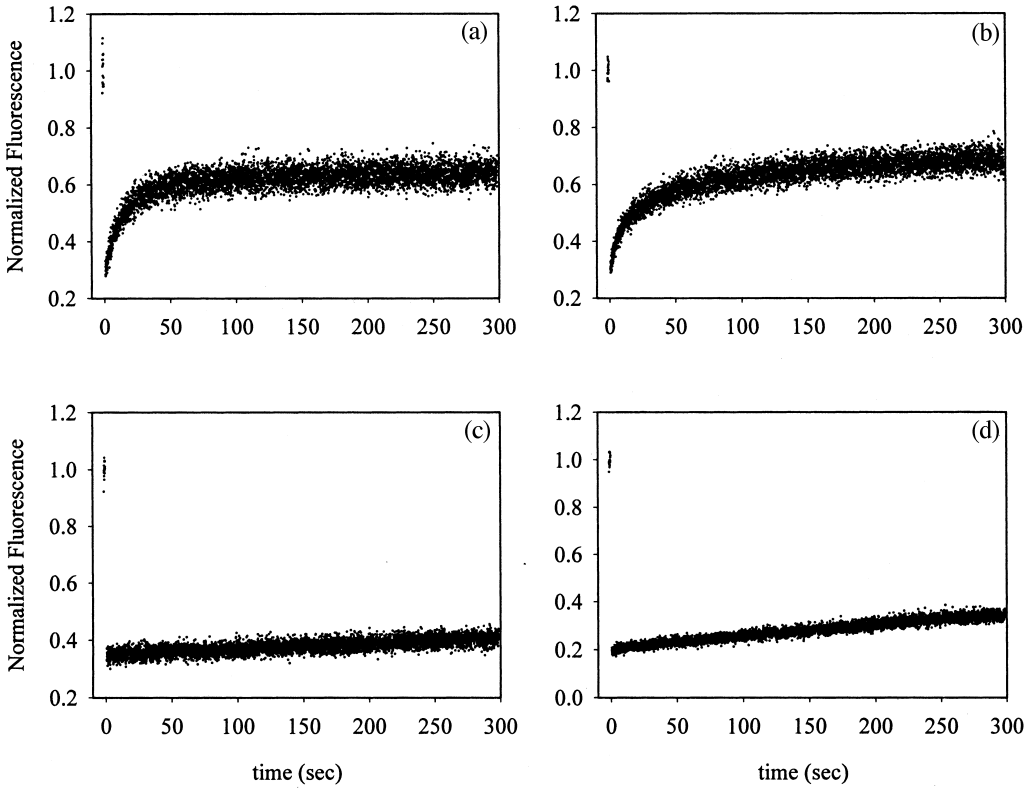

Fig. 3. FPPR data for POPC/cholesterol planar membranes. These plots show typical recovery curves for NBD-PC diffusion in planar membranes made from vesicles composed of POPC and cholesterol. The stripe period, a, is equal to (a,b) 19.5 μm or (c,d) ∞. The $1/e^2$-radius of the Gaussian shaped illuminated area is (a,c) 75 μm and (b,d) 50 μm.

across the Gaussian shape, as well as from across the stripes. However, the general expression for this condition [Eq. (16)] is not a tractable fitting form because of the large number of p-values (≥ 16) necessary for sum convergence (Fig. 2). To address this issue, simulated recovery curves were generated with Eq. (16) using $p=1$–20. Recovery curves were simulated, with the parameters s and a set to their measured values, for fractional mobilities and diffusion coefficients in the ranges of those shown in Table 1 and for bleach depths in the range 60%–85%. Simulated recovery curves were then fit to Eq. (18) [the low-bleach limit of Eq. (16)]. Curves calculated from Eq. (16) with $\mu_2=0$ were fitted to Eq. (18) with $\mu_2=0$ and α, μ_1 and D_1 as free parameters. Curves calculated from Eq. (16) with $\mu_2\neq 0$ were fitted to Eq. (18) with α, μ_1, μ_2, D_1 and D_2 as free parameters. Resulting best-fits yielded values of α and $D_{1,2}$ within $<10\%$ and values of $\mu_{1,2}$ within $<15\%$ of the values used to simulate the data. Simulated recovery curves representing a single diffusing species [Eq. (16) with $\mu_2=0$] were not artifactually fit by the two component model [Eq. (18) with $\mu_2\neq 0$] under any of the conditions evaluated. These simulations indicate that Eq. (18) is a reasonable approximation to Eq. (16) even for rather deep bleached fractions.

4.5. FPPR data in the absence of the ruling

Recovery curves obtained in the absence of the ruling ($k=0$) were fitted to Eq. (20) with α and $\mu_1\lambda$ as free parameters, and to Eq. (19) with α,

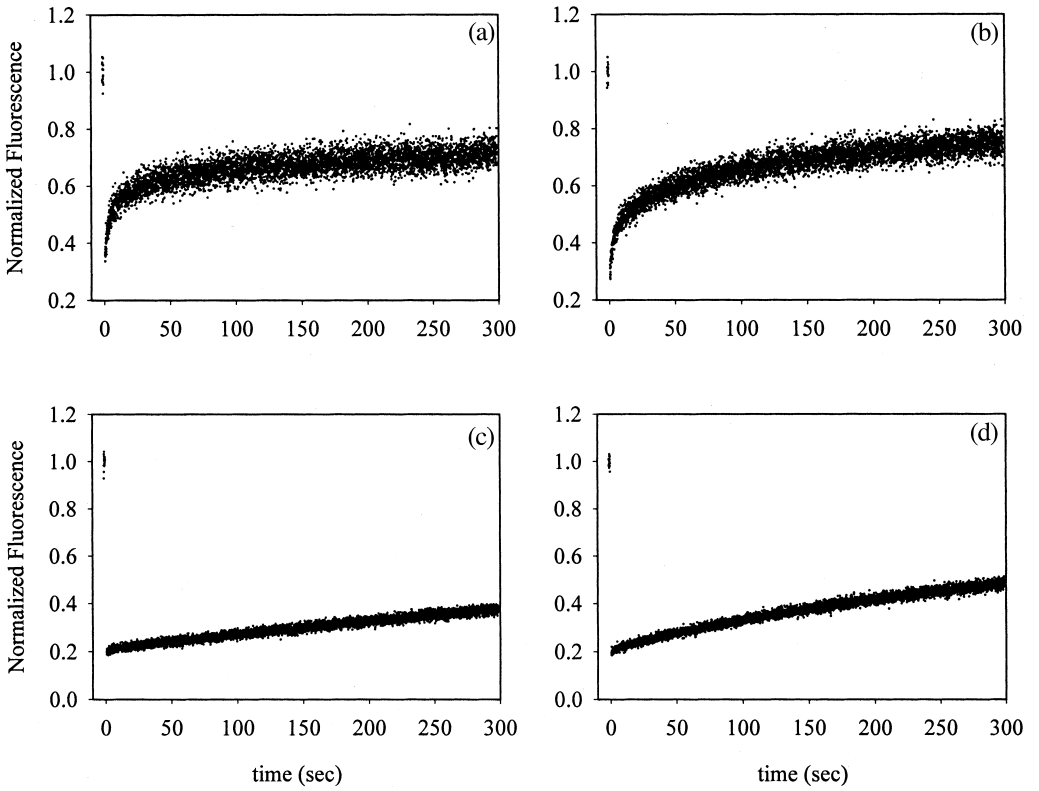

Fig. 4. FPPR data for POPC planar membranes. These plots show typical recovery curves for NBD-PC diffusion in planar membranes made from vesicles composed of POPC. The stripe period, a, is (a,b) 19.5 μm or (c,d) ∞. The $1/e^2$-radius of the Gaussian shaped illuminated area is (a,c) 75 μm and (b,d) 50 μm.

μ_1 and λ as free parameters (Fig. 7). Data acquired over 35 s were adequately fit by Eq. (20) ($\chi^2_{red} < 1$), but data acquired over 5 min required Eq. (19) for all sample types. For all sample types, the average product $\mu_1\lambda$ obtained by fitting the shorter time data to Eq. (20) and the longer time data to Eq. (19) were equivalent within experimental error. Diffusion coefficients (D_1), obtained from values of λ, corresponding to the best-fits of the 5-min acquisition time data, were consistent with those obtained from the best-fits to similar FPPR curves obtained with the ruling in place. The measured values of $\mu_1\lambda$ are shown in Table 2. The ratios of the values of these products for the two beam sizes are ≈ 2.0 and are equivalent, within experimental uncertainty, to the square of the beam size ratio (2.2 ± 0.2), given a 5% error in the measurement of s.

4.6. Analysis of FPPR data using the low bleach limit for a beam of finite extent intersected by a ruling

Recovery curves were fit to the model representing a single diffusing species [Eq. (18), $\mu_2 = 0$] with α, D_1 and μ_1 as free parameters. The product $\mu_1\lambda$ was set to the average value determined from the recovery data taken with no ruling (Table 2). This theoretical form fit the short time data for the POPC/cholesterol samples moderately well, but there was no improvement over fits to Eq. (15) with $q = 1$ (Fig. 5a,e). Similarly, there

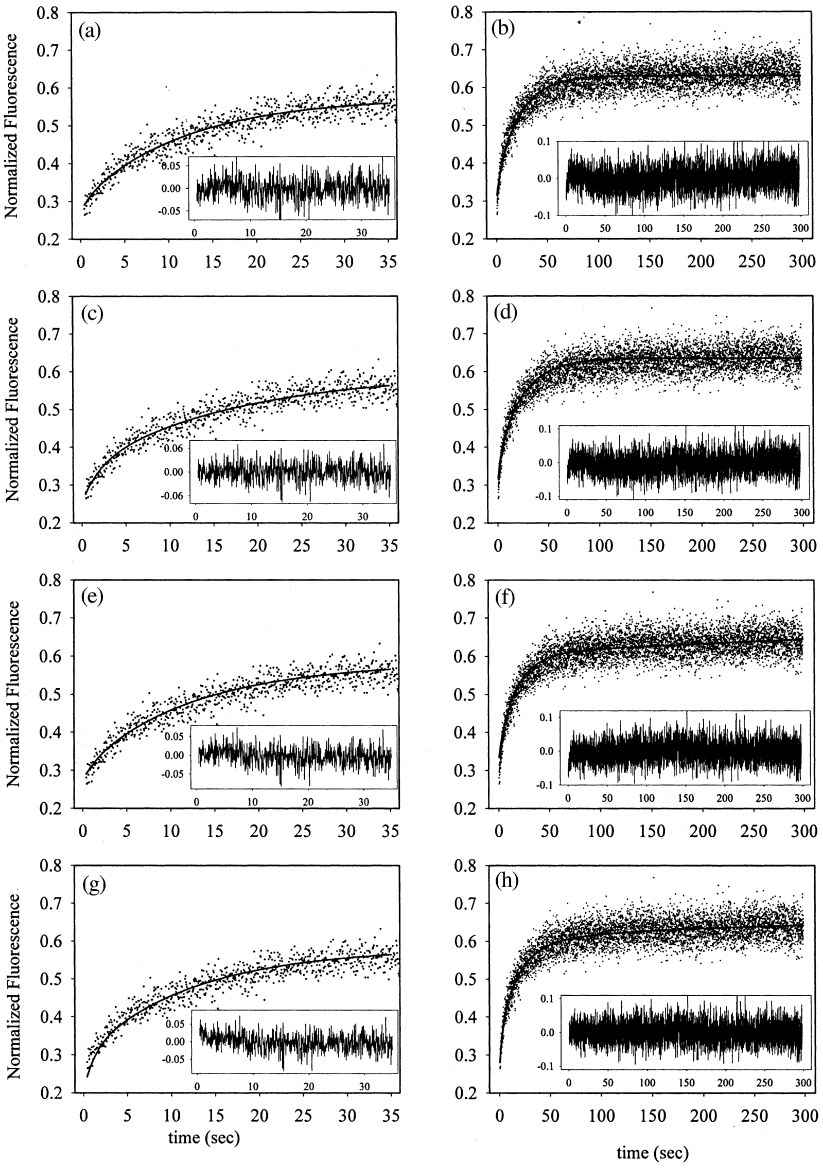

Fig. 5. Best-fits of FPPR data to theoretical forms for POPC/cholesterol planar membranes. A typical recovery curve for NBD-PC diffusion in a planar membrane made from vesicles composed of POPC and cholesterol is shown along with the best-fits to different theoretical forms. The acquisition time was (a,c,e,g) 35 s and (b,d,f,h) 5 min. The curve was fitted to (a,b) Eq. (15) with $q=1$; (c,d) Eq. (15) with $q=2$; (e,f) Eq. (18) with $\mu_2=0$; and (g,h) Eq. (18). Free parameters were (a,b,e,f) α or β, D_1 and μ_1; (c,d,g,h) α or β, D_1, D_2, μ_1 and μ_2. For (e–h), the product $\mu_1\lambda$ in Eq. (18) was fixed at its average value as determined by fitting the recovery data with no ruling. In all fits, the $1/e^2$-radius of the Gaussian-shaped illuminated area and the stripe period were $s=75$ μm and $a=19.5$ μm. Best-fit values and χ^2_{red} are: (a) $\beta=0.76$, $D_1=8.01\times10^{-9}$ cm^2/s, $\mu_1=0.88$ and $\chi^2_{red}=0.85$; (b) $\beta=0.73$, $D_1=4.31\times10^{-9}$ cm^2/s, $\mu_1=0.99$ and $\chi^2_{red}=1.05$; (c) $\beta=0.79$, $D_1=4.33\times10^{-8}$ cm^2/s, $D_2=5.59\times10^{-9}$ cm^2/s, $\mu_1=0.19$, $\mu_2=0.79$ and $\chi^2_{red}=0.84$; (d) $\beta=0.73$, $D_1=2.36\times10^{-8}$ cm^2/s, $D_2=3.91\times10^{-9}$ cm^2/s, $\mu_1=0.09$, $\mu_2=0.91$ and $\chi^2_{red}=1.03$; (e) $\beta=0.76$, $D_1=8.17\times10^{-9}$ cm^2/s, $\mu_1=0.86$ and $\chi^2_{red}=0.85$; (f) $\beta=0.71$, $D_1=5.36\times10^{-9}$ cm^2/s, $\mu_1=0.89$ and $\chi^2_{red}=1.01$; (g) $\beta=0.84$, $D_1=8.07\times10^{-8}$ cm^2/s, $D_2=8.13\times10^{-9}$ cm^2/s, $\mu_1=0.19$, $\mu_2=0.78$ and $\chi^2_{red}=1.06$; and (h) $\beta=0.78$, $D_1=2.26\times10^{-8}$ cm^2/s, $D_2=4.05\times10^{-9}$ cm^2/s, $\mu_1=0.31$, $\mu_2=0.69$ and $\chi^2_{red}=0.98$.

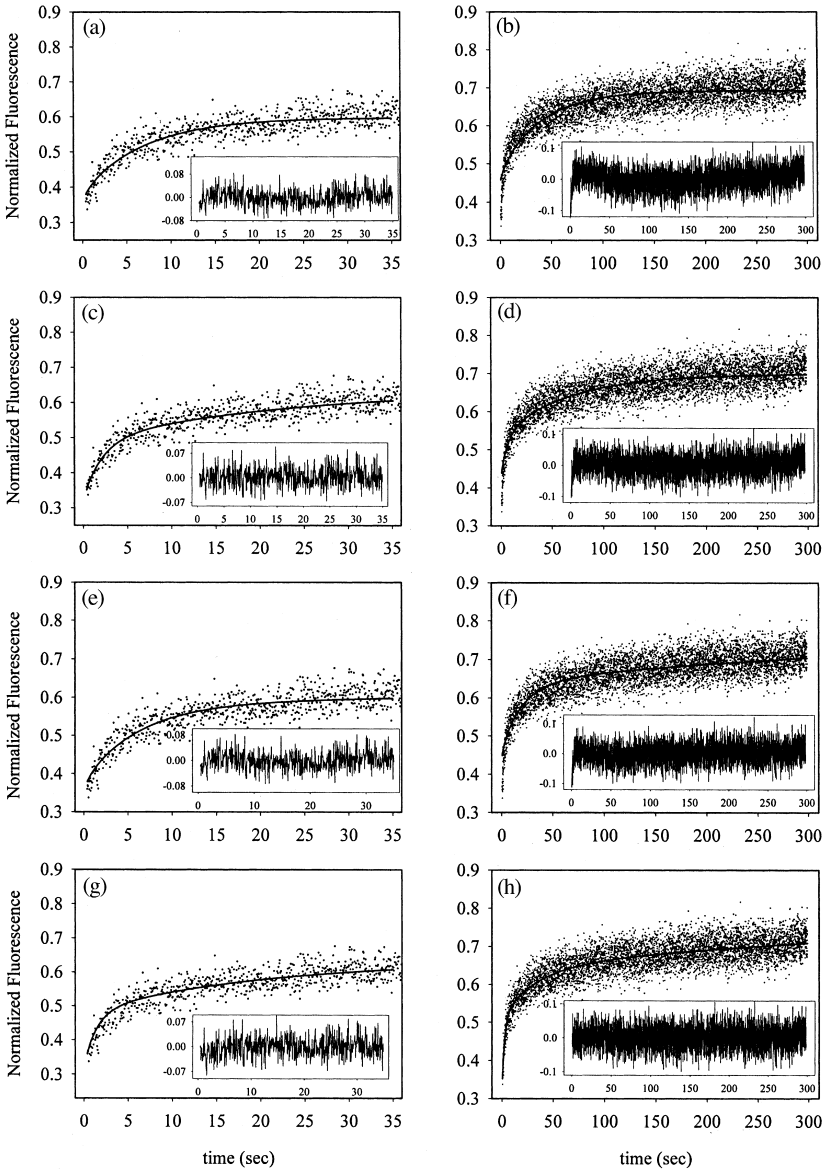

Fig. 6. Best-fits of FPPR data to theoretical forms for POPC planar membranes. A typical recovery curve for NBD-PC diffusion in a planar membrane made from vesicles composed of POPC is shown along with the best-fits to different theoretical forms. The acquisition time was (a,c,e,f) 35 s and (b,d,f,h) 5 min. The curve was fit to (a,b) Eq. (15) with $q=1$; (c,d) Eq. (15) with $q=2$; (e,f) Eq. (18) with $\mu_2=0$; and (g,h) Eq. (18). Free parameters were (a,b,e,f) α or β, D_1 and μ_1; (c,d,g,h) α or β, D_1, D_2, μ_1 and μ_2. For (e–h), the product $\mu_1\lambda$ in Eq. (18) was fixed at its average value, as determined by fitting the recovery data with no ruling. In all fits, the $1/e^2$-radius of the Gaussian-shaped illuminated area and the stripe period were $s=75$ μm and $a=19.5$ μm. Best-fit values and χ^2_{red} are (a) $\beta=0.66$, $D_1=1.35\times10^{-8}$ cm^2/s, $\mu_1=0.79$ and $\chi^2_{red}=1.01$; (b) $\beta=0.57$, $D_1=2.35\times10^{-9}$ cm^2/s, $\mu_1=0.93$ and $\chi^2_{red}=1.18$; (c) $\beta=0.73$, $D_1=4.53\times10^{-8}$ cm^2/s, $D_2=4.23\times10^{-9}$ cm^2/s, $\mu_1=0.50$, $\mu_2=0.50$ and $\chi^2_{red}=0.94$; (d) $\beta=0.60$, $D_1=1.35\times10^{-8}$ cm^2/s, $D_2=1.44\times10^{-9}$ cm^2/s, $\mu_1=0.33$, $\mu_2=0.66$ and $\chi^2_{red}=1.06$; (e) $\beta=0.67$, $D_1=1.50\times10^{-8}$ cm^2/s, $\mu_1=0.77$ and $\chi^2_{red}=1.00$; (f) $\beta=0.58$, $D_1=4.63\times10^{-9}$ cm^2/s, $\mu_1=0.76$ and $\chi^2_{red}=1.05$; (g) $\beta=0.73$, $D_1=6.96\times10^{-8}$ cm^2/s, $D_2=5.38\times10^{-9}$ cm^2/s, $\mu_1=0.48$, $\mu_2=0.46$ and $\chi^2_{red}=0.98$; and (h) $\beta=0.73$, $D_1=3.75\times10^{-8}$ cm^2/s, $D_2=5.38\times10^{-9}$ cm^2/s, $\mu_1=0.57$, $\mu_2=0.42$ and $\chi^2_{red}=0.99$.

Table 1
Diffusion coefficients and fractional mobilities as determined by the best-fits of FPPR data for short acquisition times to the theoretical form for infinite beam size

Beam radius (s) (μm)	100 μ_1	D_1 (10^{-8} cm^2 s^{-1})	100 μ_2	D_2 (10^{-8} cm^2 s^{-1})	χ^2_{red}
POPC/cholesterol[a]					
75	81 (1)	0.71 (0.01)	–	–	0.93 (0.01)
50	78 (1)	0.74 (0.01)	–	–	0.96 (0.01)
POPC[b]					
75	48 (3)	3.95 (0.26)	48 (6)	0.45 (0.05)	0.99 (0.02)
50	40 (1)	3.89 (0.13)	59 (1)	0.39 (0.03)	0.96 (0.01)

The acquisition time was 35 s, and the stripe periodicity was $a=19.5$ μm. The numbers in parentheses represent standard deviations (S.D.) of the means, and averages are over three different samples and 15 curves.

[a] The values represent best-fits to Eq. (15) with $q=1$ and β, μ_1 and D_1 as free parameters.

[b] The values represent best-fits to Eq. (15) with $q=2$ and β, μ_1, μ_2, D_1 and D_2 as free parameters.

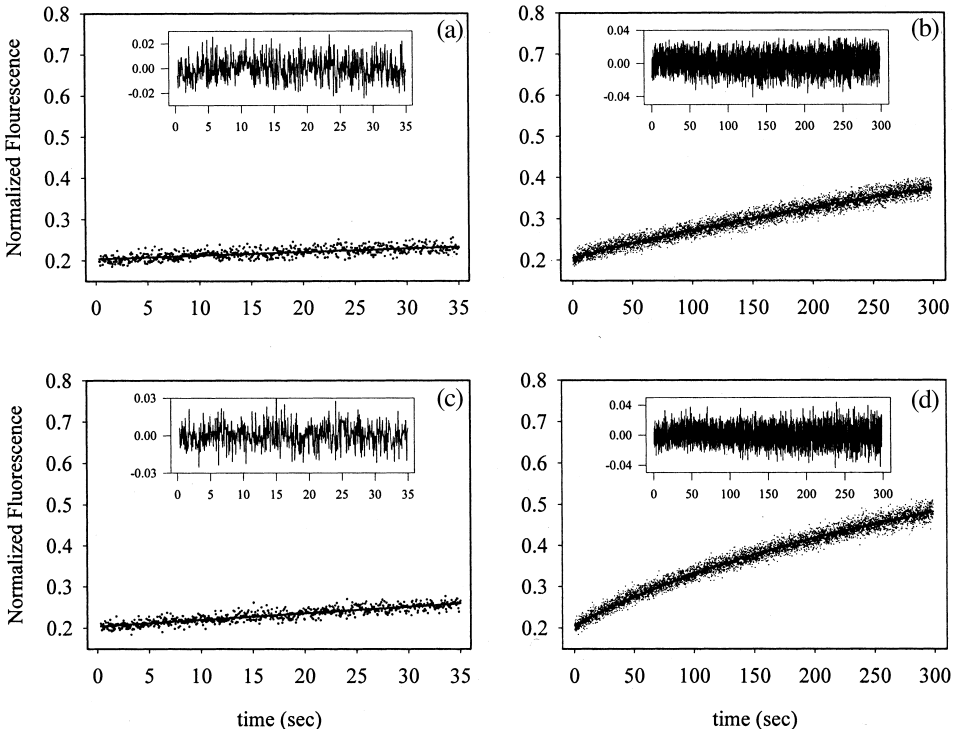

Fig. 7. Best-fits of fluorescence photobleaching recovery data to theoretical forms for an infinite stripe period. Recovery curves for NBD-PC diffusion in planar membranes made from (a,b) POPC and cholesterol and (c,d) POPC were acquired in the absence of the Ronchi ruling ($a=\infty$ and $k=0$). The $1/e^2$-radius of the Gaussian-shaped illuminated area was $s\approx 75$ μm. These data were fitted to Eq. (20) with α and $\mu_1\lambda$ as free parameters (a,c) or Eq. (19) with α, μ_1 and λ as free parameters (b,d). Best-fit values and χ^2_{red} are (a) $\alpha=4.99$, $\mu_1\lambda=1.0\times10^{-3}$ s^{-1} and $\chi^2_{red}=0.99$; (b) $\alpha=4.99$, $\mu_1=0.93$, $\lambda=1.0\times10^{-3}$ s^{-1} ($\mu_1\lambda=0.93\times10^{-3}$ s^{-1}) and $\chi^2_{red}=0.99$; (c) $\alpha=4.99$, $\mu_1\lambda=2.0\times10^{-3}$ s^{-1} and $\chi^2_{red}=0.96$; and (d) $\alpha=4.99$, $\mu_1=0.90$ and $\lambda=2.1\times10^{-3}$ s^{-1} ($\mu_1\lambda=1.9\times10^{-3}$ s^{-1}) and $\chi^2_{red}=0.97$.

Table 2
Diffusion coefficients and fractional mobilities as determined by the best-fits of FPPR data to the theoretical form for two diffusing components and a finite beam size intersected by a ruling

Beam radius (s) (μm)	$\mu_1\lambda$ (10^{-3} s^{-1})	100 μ_1	D_1 (10^{-8} cm^2 s^{-1})	100 μ_2	D_2 (10^{-8} cm^2 s^{-1})	χ^2_{red}
POPC and cholesterol						
75	0.57 (0.02)	41 (2)	1.47 (0.05)	55 (2)	0.29 (0.02)	0.99 (0.01)
50	1.14 (0.03)	49 (2)	1.17 (0.05)	46 (2)	0.18 (0.01)	0.99 (0.01)
POPC						
75	1.04 (0.01)	60 (4)	3.42 (0.37)	37 (4)	0.31 (0.10)	0.99 (0.01)
50	2.04 (0.03)	60 (4)	3.12 (0.25)	39 (4)	0.27 (0.09)	1.00 (0.01)

The acquisition time was 5 min, and the stripe periodicity was $a = 19.5$ μm. The numbers in parentheses represent S.D. of the means, and averages are over three different samples and 15 curves.

was no significant improvement in the fits of short time POPC data to Eq. (18) with $\mu_2 = 0$ as compared to Eq. (15) with $q = 2$ (Fig. 6c,e). At longer times, Eq. (18) with $\mu_2 = 0$ did not adequately represent any of the sample types as indicated by the χ^2_{red} values in the range of 1.0–1.2 where higher values correspond to samples with faster diffusion and/or smaller observation areas (Fig. 5f and Fig. 6f).

Recovery curves were next fit to Eq. (18) with α, D_1, D_2, μ_1 and μ_2 as free parameters, and $\mu_1\lambda$ set to its determined value. This theoretical form adequately fit all four sample types, measured over the longer acquisition time. The use of this form is statistically justified over the form for a single diffusing species [Eq. (18), $\mu_2 = 0$] as indicated by *F*-statistic values in the range of 20–400. Similarly, *t*-test analysis confirmed that the χ^2-goodness-of-fit parameters, representing the best-fits to Eqs. (18) and (15) with $q = 2$, were different with 95–98% certainty, and χ^2_{red} representing Eq. (18) were lower for all sample types. The best-fit parameters and χ^2_{red} values for fits to Eq. (18) are shown in Table 2. The best-fit values obtained for the diffusion coefficients and fractional mobilities in membranes composed of POPC were approximately consistent with those obtained from fits of the shorter duration data to Eq. (15) with $q = 2$ (Table 1) as well as with previous results [14]. On the contrary, longer duration FPPR curves for the cholesterol-containing membranes demonstrated non-ideal diffusion, better described by a two-component model, unlike the shorter duration data, which were described well by Eq. (15) with $q = 1$. Data acquired over the shorter acquisition time were also fit to this model, but there was no improvement in χ^2_{red} as compared to fits to Eq. (15).

5. Discussion

When probed with FPPR over short acquisition times (Table 1), the fluorescent lipid probe NBD-PC exhibits multi-component diffusion in planar membranes composed of POPC. For the same experimental conditions, data for this probe in POPC/cholesterol planar membranes are adequately described by a single diffusing component, but the apparent mobile fractions are significantly less than one (Table 1). Because of the apparent presence of this immobile fraction, as well as the magnitude of the slower diffusion coefficients observed for POPC membranes, it is necessary to acquire data over longer time periods (5 min). However, significant recovery is observed over this longer time period in the absence of the Ronchi ruling, and in the presence of the ruling, the fluorescence recovers to a value corresponding to greater than one-half of the bleached fluorescence (Figs. 3 and 4). These effects are most likely due to exchange of bleached and unbleached molecules through the spatial intensity gradient of the Gaussian-shaped beam rather than through the striped regions created by the Ronchi ruling. This difficulty cannot be accommodated by using a smaller stripe periodicity, because the recovery

times for the more rapidly diffusing component through the stripes is not much larger than the minimum bleach time required by using standard argon ion laser powers. Therefore, a theoretical formalism, which accounts for contributions to the recovery curves from the larger, Gaussian-shaped spatial profile of the excitation intensity [Eqs. (2) and (3)], is required.

A general solution for FPPR recovery curves when the excitation intensity is the product of a circular Gaussian and a linear square wave (Fig. 1a) is given in Eqs. (6)–(8) for a single diffusing component. The shape of the fluorescence recovery is not a simple sum or product of two functions which reflect the two features (beam shape and ruling) giving rise to the spatial dependence of the intensity. A simpler approximation to the general solution, shown in Eqs. (6)–(8), which is applicable when the $1/e^2$-radius of the beam is only slightly larger than the stripe periodicity, is given in Eq. (14). In practice, the signal-to-noise ratio is usually such that FPPR data can be adequately described by two components with different diffusion coefficients and an immobile component. Typical signal-to-noise ratios do not usually accommodate a third mobile component. In the case where only the more rapidly diffusing component contributes to fluorescence recovery via motion through the overall Gaussian shape of the beam and $\sigma > 1$, the shape of the fluorescence recovery is given by Eq. (16). This function is not simple for non-linear curvefitting, because the sum over the integer p does not rapidly converge. However, numerical simulations indicated that retaining only the $p = 1$ term (the low-bleach limit) was adequate for typical experimental conditions. This further approximation [Eq. (18)] was used for subsequent data analysis.

The new formalism for analyzing longer acquisition time FPPR data adequately described the translational mobility of a fluorescent lipid in both POPC and POPC/cholesterol planar membranes (Table 2). For POPC membranes, best-fit values of the diffusion coefficients and fractions of each mobile species were equivalent within experimental error when comparing results for the two different observation beam radii. For POPC/cholesterol membranes, the values were approximately equivalent. The best-fit values describing diffusion in the POPC membranes obtained over the shorter acquisition time fitted to Eq. (15) with $q = 2$ (Table 1) and those obtained over the longer duration fit to Eq. (18) (Table 2) are in good agreement. On the contrary, FPPR curves representing the POPC/cholesterol membranes were well described by a single diffusing component for the shorter acquisition time (Table 1), but heterogeneous behavior was observed at the longer acquisition time (Table 2). The diffusion coefficients and fractional mobilities shown in Tables 1 and 2 are in the same range as those previously reported [14,18–20].

The data demonstrate that the translational mobility of lipids in supported membranes may be adequately described by the new theoretical formalism described here. This formalism might be applicable not only to lipids in planar membranes, but also to proteins in or bound to planar membranes [21,22], molecules in polymer films [23–25], polymers in liquid crystalline solutions [26] and proteins in intact cell membranes [27–31]. With minor theoretical adaptations, the formalism might also be applicable to fringe FPPR [21,22,27–32], in which the pattern is formed by the interference of two different beams rather than with a Ronchi ruling.

Acknowledgments

We would like to thank Craig Loehle of Loehle Enterprises for assistance with adapting the available Mathematica data analysis routine to our application. This work was supported by NSF Grant MCB-0130589.

Appendix A: Expansions and sums

The coefficients c_n sum as follows:

$$\sum_{n\ \mathrm{odd}} c_n = \sum_{m,n\ \mathrm{odd}} c_m c_n = 1$$
$$\frac{1}{2}\sum_{n\ \mathrm{odd}} c_n^2 = \frac{8}{\pi^2}\sum_{n\ \mathrm{odd}} \frac{1}{n^2} = 1 \qquad \text{(A1)}$$

Deriving the general expression for $F(t)$ [Eqs. (6)–(8)] requires the following expansion:

$$e^{-\kappa I(x,y)} = \sum_{p=0}^{\infty} \frac{(-\kappa I_0)^p}{p!} \exp\left[-\frac{2p(x^2+y^2)}{s^2}\right] \times \left\{\frac{1}{2}\left[1+\sum_{n\ \mathrm{odd}}^{\infty} c_n \cos(nkx)\right]\right\}^p \quad \text{(A2)}$$

Because the last factor in Eq. (A2) is a square wave with magnitude ranging from zero to one:

$$\left[1+\sum_{n\ \mathrm{odd}}^{\infty} c_n \cos(nkx)\right]^p = 2^{p-1}\left[1+\sum_{n\ \mathrm{odd}}^{\infty} c_n \cos(nkx)\right] \quad p>0 \quad \text{(A3)}$$

Derivation of the bleached fraction β [Eq. (10)] requires the following sum:

$$\sum_{m,n\ \mathrm{odd}} c_m c_n \left\{\exp\left[-\frac{(m+n)^2}{1+p}\sigma\right] + \exp\left[-\frac{(m+n)^2}{1+p}\sigma\right]\right\} = 2 \quad \text{(A4)}$$

References

[1] W.L.C. Vaz, Z.I. Derzko, K.A. Jacobson, Photobleaching measurements of the lateral diffusion of lipids and proteins in artificial phospholipid bilayer membranes, Cell Surf. Rev. 8 (1982) 83–135.

[2] E.L. Elson, Fluorescence correlation spectroscopy and photobleaching recovery, Annu. Rev. Phys. Chem. 36 (1985) 379–406.

[3] Y.I. Henis, Fluorescence photobleaching recovery to probe virus–cell fusion and virus-mediated cell fusion, Meth. Enzymol. 220 (1993) 350–362.

[4] J.M. Kovaleski, M.J. Wirth, Applications of fluorescence recovery after photobleaching, Anal. Chem. 69 (1997) A600–A605.

[5] T.K.L. Meyvis, S.C. De Smedt, P. Van Oostveldt, J. Demeester, Fluorescence recovery after photobleaching: a versatile tool for mobility and interaction measurements in pharmaceutical research, Pharmaceut. Res. 16 (1999) 1153–1162.

[6] D. Axelrod, D.E. Koppel, J. Schlessinger, E.L. Elson, W.W. Webb, Mobility measurement by analysis of fluorescence photobleaching recovery kinetics, Biophys. J. 16 (1976) 1055–1069.

[7] D.E. Koppel, D. Axelrod, J. Schlessinger, E.L. Elson, W.W. Webb, Dynamics of fluorescence marker concentration as a probe of mobility, Biophys. J. 16 (1976) 1315–1329.

[8] B.A. Smith, H.M. McConnell, Determination of molecular motion in membranes using periodic pattern photobleaching, Proc. Natl. Acad. Sci. USA 75 (1978) 2759–2763.

[9] Z.P. Huang, K.H. Pearce, N.L. Thompson, Effect of bovine prothrombin fragment 1 on the translational diffusion of phospholipids in Langmuir–Blodgett monolayers, Biochim. Biophys. Acta 1112 (1992) 259–265.

[10] R.M. Clegg, W.L.C. Vaz, Progress in protein–lipid interactions, in: A. Watts, J.J.H.H.M. de Pont (Eds.), Translational Diffusion of Proteins and Lipids in Artificial Lipid Bilayer Membranes: A Comparison of Experiment with Theory, Elsevier Science Publishers, Holland, 1985, pp. 173–229.

[11] K. Beck, Cytomechanics, in: L.J. Bereiter-Hahn, O.R. Anderson, W.-E. Reif (Eds.), Mechanical Concepts of Membrane Dynamics: Diffusion and Phase Separation in Two Dimensions, Springer-Verlag, Berlin–Heidelberg, 1987, pp. 79–99.

[12] F. Zhang, G.M. Lee, K. Jacobson, Protein lateral mobility as a reflection of membrane microstructure, BioEssays 15 (1993) 579–588.

[13] J.-F. Tocanne, L. Dupou-Cezanne, A. Lopez, Lateral diffusion of lipids in model and natural membranes, Progress Lipid Res. 33 (1994) 203–237.

[14] T.E. Starr, N.L. Thompson, Formation and characterization of planar phospholipid bilayers supported on TiO_2 and $SrTiO_3$ single crystals, Langmuir 16 (2000) 10301–10308.

[15] F. Lanni, B.R. Ware, Modulation detection of fluorescence photobleaching recovery, Rev. Sci. Instrum. 53 (1982) 905–908.

[16] L.L. Wright, A.G. Palmer, N.L. Thompson, Inhomogeneous translational diffusion of monoclonal antibodies on phospholipid Langmuir–Blodgett films, Biophys. J. 54 (1988) 463–470.

[17] D.E. Koppel, M.P. Sheetz, A localized pattern photobleaching method for the concurrent analysis of rapid and slow diffusion processes, Biophys. J. 43 (1983) 175–181.

[18] E. Kalb, S. Frey, L.K. Tamm, Formation of supported planar bilayers by fusion of vesicles to supported phospholipid monolayers, Biochim. Biophys. Acta 1103 (1992) 307–316.

[19] B.J. Balcom, N.O. Petersen, Lateral diffusion in model membranes is independent of the size of the hydrophobic region of molecules, Biophys. J. 65 (1993) 630–637.

[20] G.J. Schutz, H. Schindler, T. Schmidt, Single molecule microscopy on model membranes reveals anomalous diffusion, Biophys. J. 73 (1997) 1073–1080.

[21] Z.P. Huang, N.L. Thompson, Theory for 2-photon excitation in pattern photobleaching with evanescent illumination, Biophys. Chem. 47 (1993) 241–249.
[22] Z.P. Huang, K.H. Pearce, N.L. Thompson, Translational diffusion of bovine prothrombin fragment 1 weakly bound to supported planar membranes: measurement by total internal reflection with fluorescence pattern photobleaching recovery, Biophys. J. 67 (1994) 1754–1766.
[23] B.A. Smith, Measurement of diffusion in polymer-films by fluorescence redistribution after pattern photobleaching, Macromolecules 15 (1982) 469–472.
[24] Z.H. Yang, J.A. Galloway, H.U. Yu, Protein interactions with poly(ethylene glycol) self-assembled monolayers on glass substrates: diffusion and adsorption, Langmuir 15 (1999) 8405–8411.
[25] K.C. Tseng, N.J. Turro, C.T. Durning, Molecular mobility in polymer thin films, Phys. Rev. E 61 (2000) 1800–1811.
[26] P.S. Russo, M. Baylis, Z.M. Bu, et al., Self-diffusion of a semiflexible polymer measured across the lyotropic liquid–crystalline-phase boundary, J. Chem. Phys. 111 (1999) 1746–1752.
[27] J.M.E.H. Chahine, S. Cribier, P.F. Devaux, Phospholipid transmembrane domains and lateral diffusion in fibroblasts, Proc. Natl. Acad. Sci. USA 90 (1993) 447–451.
[28] H.M. Munnelly, D.A. Roess, W.F. Wade, B.G. Barisas, Interferometric fringe fluorescence photobleaching recovery interrogates entire cell surfaces, Biophys. J. 75 (1998) 1131–1138.
[29] D.A. Roess, R.D. Horvat, H. Munnelly, B.G. Barisas, Luteinizing hormone receptors are self-associated in the plasma membrane, Endocrinol. 141 (2000) 4518–4523.
[30] G. Foucault, M. Vacher, S. Cribier, M. Arrio-Dupont, Interactions between β-enolase and creatine kinase in the cytosol of skeletal muscle cells, Biochem. J. 346 (2000) 127–131.
[31] M. Arrio-Dupont, G. Foucault, M. Vacher, P.F. Devaux, S. Cribier, Translational diffusion of globular proteins in the cytoplasm of cultured muscle cells, Biophys. J. 78 (2000) 901–907.
[32] J.L. Robeson, R.D. Tilton, Effect of concentration quenching on fluorescence recovery after photobleaching measurements, Biophys. J. 68 (1995) 2145–2155.